

Single-Star H II Regions as a Probe of Massive Star SEDs

Jordan Zastrow¹, M.S. Oey¹ and E.W. Pellegrini¹

¹ Department of Astronomy, 500 Church Street, University of Michigan, Ann Arbor, MI, 48109, USA

Abstract: We critically examine stellar atmosphere models by exploiting the strong dependence of H II region optical spectra on the SED of the ionizing source. To accomplish this, we compare spatially resolved, longslit observations of LMC single-star H II regions to photoionization simulations based on observed nebular and stellar properties. We select stellar atmosphere models from the CoStar (Schaerer & de Koter, 1997), TLUSTY (Lanz & Hubeny, 2003), WM-basic (Pauldrach et al. 2001) and Smith et. al. (2002) grids to define the ionizing source in our simulations. Gas density fluctuations are necessary to simultaneously fit the emission from high and low excitation ions. We evaluate the atmospheres relative to each other and overall, find atmosphere models using the WM-basic code have the best agreement with our observations.

1 Introduction

Studies of massive star feedback, stellar populations and abundances, and star formation rate indicators depend on the spectral energy distributions (SED) and derived properties of massive stars. However, these stars emit a majority of their flux at wavelengths relatively inaccessible to observations. Thus, stellar atmosphere models are an important tool for understanding fundamental galaxy properties.

Modeling massive star atmospheres is complex. To accurately represent the SED, important physics such as non-LTE conditions, the effects of line-blanketing and, wind-blanketing effects need to be included. Incorporating all these processes in detail is computationally expensive. Therefore, research groups optimize computing time by using approximate treatments for different components. For example, CoStar (Schaerer & de Koter 1997) and WM-basic (Pauldrach, Hoffman & Lennon 2001) take into account expanding atmospheres while TLUSTY (Lanz & Hubeny 2003) uses a plane-parallel one. Additionally, the treatment of line-blanketing differs from code to code. These different approaches lead to differences in the predicted SEDs. Thus, it is crucial to understand how well these model atmospheres represent the actual SEDs of the stars.

The optical emission from an H II region depends primarily on the SED of the ionizing source, the metallicity (Z), and the ionization parameter (U) which depends on the rate of ionizing photons, the gas density and morphology. If the metallicity and ionization parameter can be constrained, we can use the line emission to constrain the SED of the ionizing star.

We can accomplish this with our sample of single-star H II regions in the Large Magellanic Cloud (LMC). The LMC is an ideal location for this study because it has a well measured metallicity, a known distance and does not have the extinction and crowding issues that a Galactic study would have. Additionally, the H II regions span 20'' - 30'' in diameter which allows us to obtain spatially

Table 1: Stellar and nebular properties.

Name	SpT	Log($\frac{L}{L_{\odot}}$)	Nebula Radius (pc)	Filling Factor	High Density		Low Density	
					n_H (cm $^{-3}$)	Thickness (pc)	n_H (cm $^{-3}$)	Thickness (pc)
DEM 08c	O5.5V	4.81 \pm 0.05	6.8 \pm 1	0.03	500	0.05	1	2.0
DEM 026	O8V	4.68 \pm 0.05	6.1 \pm 0.9	0.087	80	0.25	10	1.75
DEM 020	O8V	5.08 \pm 0.05	8.5 \pm 1.2	0.137	80	0.15	1	0.9

resolved spectra. The real strength of our data set lies in the single-star nature of the H II regions. With just one ionizing source, the morphology of the nebula is much simplified. Narrowband [O III], H α , and [S II] images from the Magellanic Clouds Emission Line Survey (MCELS; Smith et al. 2005) of our objects show classical Strömgren sphere-like nebulae. This puts strong constraints on the gas density and morphology, thereby constraining U .

2 Observations

We report on the results obtained from three LMC H II regions: DEM L08c, DEM L026, and DEM L020. These objects are ionized by an O5.5V star, O8V star, and O8V star, respectively. Broadband (Bessell B and V) images and longslit spectra of these objects were obtained using the imaging spectrograph IMACS on the Magellan Baade Telescope at Las Campanas Observatory. The data were taken during the nights of 2008 January 29-31. The spectra have a spatial resolution of 0.44'' pixel $^{-1}$ and a spectral resolution of 0.75 Å pixel $^{-1}$ covering a total wavelength range of 3700 - 6740 Å. We used standard IRAF procedures for image and spectral reduction. The flux calibration was made using standard stars LTT 2415, LTT 3218, and LTT 1788 (Hamuy et al. 1994).

3 Models

Each H II region model is generated four times with the photoionization code CLOUDY (Ferland et al. 1998). Each time a different model atmosphere is used as the ionizing source. We then plot the ratio of predicted flux (F_{pre}) to observed flux (F_{obs}) for each emission line as a function of the ionization potential (IP) of that line. In this study we consider atmosphere models generated from different atmosphere codes: CoStar (Schaerer & de Koter 1997), TLUSTY (Lanz & Hubeny 2003), WM-basic (Pauldrach et al. 2001) and O star grid from Smith, Norris & Crowther (2002, hereafter SNC02). The models from SNC02 are generated using the WM-basic code with different fundamental stellar parameters for implementation into STARBURST99 (Leitherer et al. 1999).

To set up the model nebula, we need to specify the stellar luminosity, inner cloud radius, density, elemental abundance and stellar effective temperature (T_{eff}). The observed and calculated nebular and stellar parameters are shown in columns 2-4 of Table 1. Column 2 lists the spectral type (SpT) determined from our IMACS spectra. Column 3 lists the stellar luminosity which is calculated from the observed magnitudes using the bolometric correction from Martins, Schaerer & Hillier (2005). Column 4 contains the radial size of the nebula as measured from the MCELS narrowband H α image. Examining our objects in the MCELS images, the emission is consistent with gas close to the star. Therefore, we choose our inner cloud radius to be 0.1 pc for all models. A final size criterion is used to select successful models. We only consider models that reach the outer nebular radius measured with the MCELS data for comparison with our observations. Unfortunately, the gas densities of these

objects fall in the low density limit of the [O II] and [S II] density diagnostics. This means we only have an upper limit on the electron density of $n_e \leq 100 \text{ cm}^{-3}$. Elemental abundances are drawn from Garnett (1999) except for that of nitrogen. The nitrogen abundance is calculated using the observed [N II] / [O II] line ratio and the relation from Pérez-Montero & Díaz (2005). The final input for the H II region models is the T_{eff} which we leave as a free parameter.

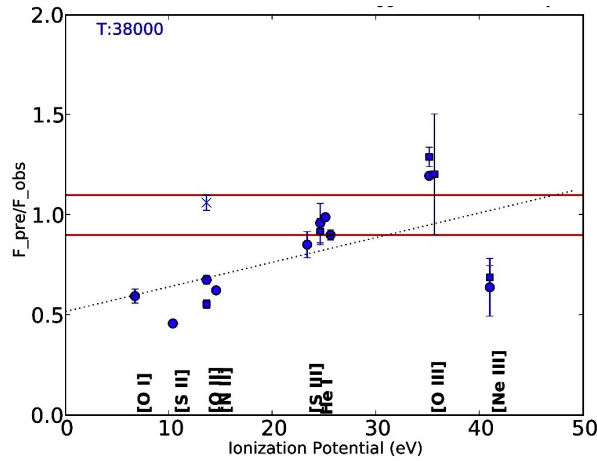


Figure 1: DEM L08c modeled as a constant density sphere with gas density of 40 cm^{-3} and using WM-basic. $F_{\text{pre}}/F_{\text{obs}}$ of emission lines is plotted as a function of IP. The red lines mark the $\pm 10\%$ allowance for agreement between the models and observations. Error bars represent the measurement error and do not include systematic error. The different symbols show $F_{\text{pre}}/F_{\text{obs}}$ for two different observations of the object and are representative of the observational scatter.

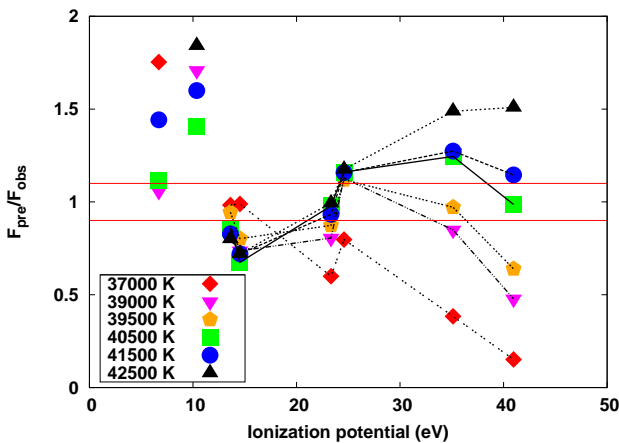


Figure 2: DEM L08c modeled using atmospheres from the SNC02 grid with 6 different T_{eff} . This plot shows that moving from low to high T_{eff} , the models first favor ions with low IP and then they favor ions with high IP.

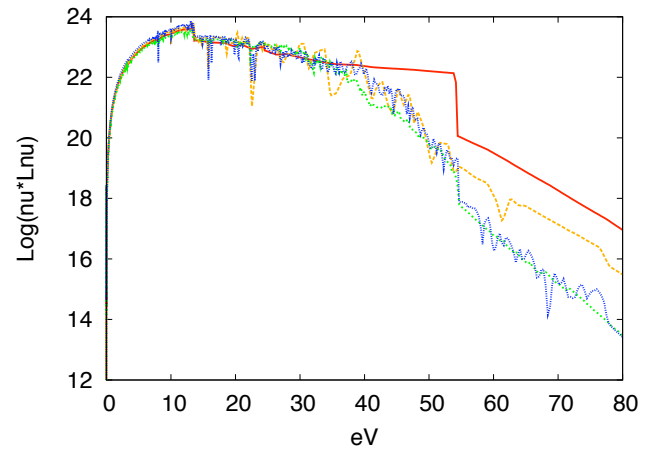


Figure 3: Comparison of the emergent SEDs from the atmospheres discussed in this paper for atmospheres with $T_{\text{eff}} = 39000$. Red, green, blue, orange correspond to CoStar (Schaerer & de Koter 1997), TLUSTY (Lanz & Hubeny 2003), WM-basic (Pauldrach et al. 2001), and Smith et al. (2002) model atmospheres, respectively.

4 Results

In our initial suite of models, we model the H II regions as single-density Strömgren spheres. While it is possible to match the predicted emission to the observed one for ions with high IP, the models

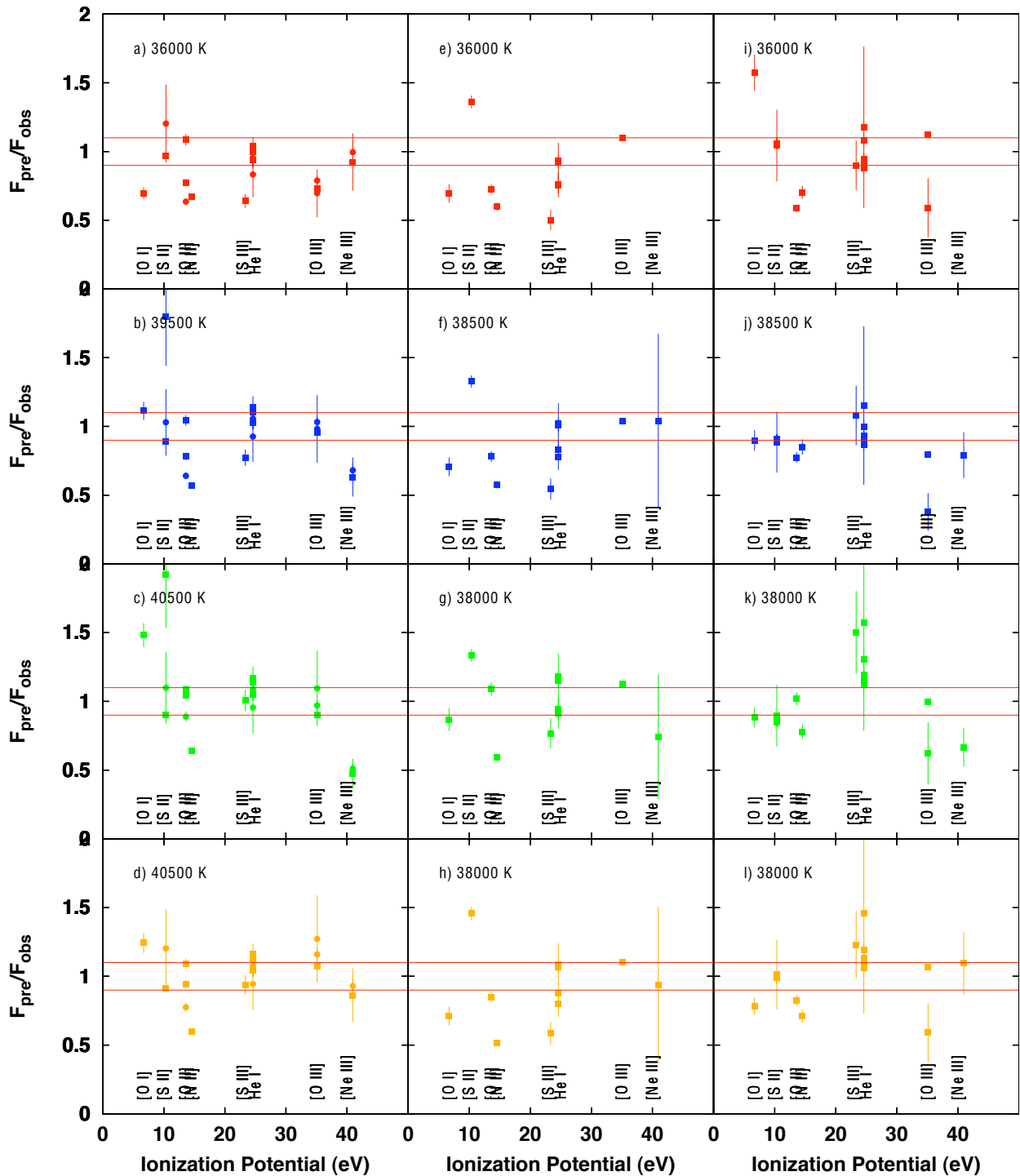


Figure 4: Same as Figure 1 except here, the each H II region is modeled as a nebula with density fluctuations. The T_{eff} of the model atmosphere is printed in the top left corner of each plot. Red, blue, green and orange points correspond to CoStar, WM-basic, TLUSTY, and SN02 model atmospheres, respectively. DEM L08c, ionized by an O5.5V, star is modeled in plots *a-d*; DEM L020, ionized by an O8V, star is modeled in plots *e-h*; DEM L026, ionized by an O8V, star is modeled in plots *i-l*.

consistently under-predict the ions with low IP (see Figure 1). This indicates the ionization parameter is too high. To reproduce the ions with low IP, we need a way to have dense gas further from the star to receive a weakened radiation field. At the same time we need to maintain the gas close to the star to reproduce the emission from ions with high IP. This is accomplished by a density distribution that has small high density clumps with a low density filler between.

The best models for our objects are shown in Figure 4. Each H II region is modeled as a uniform, low-density sphere with small regions of dense gas. The optimal model is determined by plotting the ratio of predicted to observed line flux ($F_{\text{pre}}/F_{\text{obs}}$) as a function of IP. For each atmosphere and object, we step through our grid in T_{eff} and density (see Figure 2). Most models favor either the ions with low or high IP. We choose the model that has the flattest slope, where most points have a ratio of 1. This indicates that the atmosphere model is radiating the appropriate amount of ionizing flux at both low and high energies. The model parameters are listed in columns 5-7 of Table 1. Column 5 contains the filling factor of the high density gas component. Columns 6a and 6b list the gas density and thickness, respectively, of the high density gas component. Column 7a lists the gas density of the low density component and column 7b lists the spacing between high density regions.

Generally, we find models using WM-basic and SNC02 atmospheres consistently come closest to observations. These model atmospheres have a very detailed treatment of line blanketing and include the effects of stellar winds. Models generated using the TLUSTY atmospheres also agree well for IP less than 40 eV. However, in these models [Ne III] is significantly under-predicted. This reflects the difference in SED between TLUSTY and the other models. At 40 eV, the IP of Ne^{+2} , the TLUSTY SED has lower flux than the other model atmospheres (Figure 3). The Figure also shows that the CoStar SED has a significant excess flux at high energies relative to the other atmosphere models. As a result, it is necessary to use a stellar atmosphere model with an T_{eff} a few thousand degrees cooler to match the observed emission lines in all our objects.

In conclusion, of the four atmosphere models tested, WM-basic and SNC02 consistently ionized the model H II regions that matched the observed line emission. Additionally, we find density fluctuations necessary to generate model H II regions that reproduce the observed emission line spectrum.

Acknowledgements

This research is funded by NSF grant AST-0806476. Many thanks to the LOC for the support to attend this conference.

References

- Ferland, G.J., Korista, K.T., Verner, D.A., Ferguson, J.W., Kingdon, J.B., Verner, E.M., 1998, *PASP*, 110, 749
Garnett, D. 1999, *IAUS*, 190, 266
Hamuy, M., Suntzeff, N.B., Heathcote, S.R., Walker, A.R., Gigoux, P., & Phillips, M.M, 1994, *PASP*, 106, 566
Lanz, T. & Hubeny, I., 2003, *ApJS*, 146, 417
Leitherer, C., Schaerer, D., Goldader, J.D., et al. 1999, *ApJS*, 123, 3L
Martins, F., Schaerer, D., & Hillier, D.J., 2005, *A&A*, 436, 1049
Pauldrach, A.W., Hoffman, T.L., & Lennon, M. 2001, *A&A*, 375, 161
Pérez-Montero, E., & Díaz, A.I., 2005, *MNRAS*, 361, 1063
Schaerer, D., & de Koter, A., 1997, *A&A*, 322, 598
Smith, R.C., Points, S.D., Chu, Y.-H., Winkler, P.F., Aguilera, C., Leiton, R., & MCELS Team, 2005, *AAS*, 207, 2507
Smith, L.J., Norris, R.P., & Crowther, P.A., 2002, *MNRAS*, 337, 1309
Voges, E. S., Oey, M.S., Waltherbos, R.A.M., & Wilkinson, T.M., 2008, *AJ*, 135, 1291